Published in*: "J. Phys. Chem. C*, **2012**, *116* (31), pp 16784–16799", DOI: 10.1021/jp304962w
Which should be cited to refer to this work
http://pubs.acs.org/doi/abs/10.1021/jp304962w

Orientation and Order of Xanthene Dyes in the One-Dimensional Channels of Zeolite L: Bridging the gap between experimental data and molecular behavior.

Ettore Fois†*, Gloria Tabacchi†, Gion Calzaferri‡

†Dep. of Science and High Technology, University of Insubria, and INSTM, Via Lucini 3; I-22100 Como (Italy)- Fax: (+) 39 031 2386630
‡Department of Chemistry and Biochemistry, University of Bern Freiestrasse 3, CH-3012 Bern 2 (Switzerland)

Abstract

Supramolecular organization in nano-channels is governed by both the nature of the channels and the size, shape, charge of the guests, and may also depend by the co-solvent in the host. Oxonine (Ox^+) and pyronine (Py^+) cationic dyes in zeolite L (ZL) could provide important insight on this issue, but their orientation in the composite materials is not understood yet. Theoretical modelling of Ox^+/ZL and Py^+/ZL composites indicates that the 70-80° orientation, deduced from optical microscopy data but incompatible with host-guest geometry contraints, is not stable and reveals two possible orientations for these dyes in ZL nanochannels: perpendicular or parallel to the channel axis. In the hydrated composite, corresponding to optical microscopy experiments conditions, perpendicular Ox^+/Py^+ is the favoured orientation, suggesting a larger portion of perpendicularly oriented dye molecules and a smaller fraction aligned. Optical microscopy data might therefore be re-interpreted as the vector sum of components arising from a population of molecules with non-uniform orientation. The stability order is reversed at dry conditions indicating that the organization of xantene dyes in ZL channels is governed by water. Our study explains this co-solvent-driven supramolecular organization regime, here unraveled for the first time, and highlights the role of molecular flexibility in switching the dye orientation.

Keywords: density functional calculations, supramolecular chemistry, host-guest systems, organic-inorganic hybrid composites, photochemistry, water chemistry, FRET

1. Introduction

The orientation, distribution, and packing of molecules in one-dimensional (1D) channel materials, gels, and polymers influence the photophysical and photochemical properties of these host-guest composites considerably.[1-8] Composites with intriguing properties have been synthesized by using organizing hosts with channel diameters in the order of one nanometer, such as zeolite L (ZL), $AlPO_4$-5, MFI, and also organic channel-forming hosts.[1-6, 9-17] An apparently trivial but important feature of 1D channels is that they have only two entrances. Channels can therefore be open on both sides, plugged on one side, or plugged on both sides. This plugging can be isolating or it can be partial, allowing electrons, protons, or small molecules to pass, but blocking larger objects.[3,13-17] 1D channels can act as ordering nano-containers as explained in Figure 1 where different arrangements and orientations of molecules are illustrated. We discuss situations where the "optical electrons" associated with the individual guests preserve essentially their individual character. This does not exclude covalent bonding between the chromophores but means that no orbital overlap between them has to be considered. The double arrows in Figure 1 indicate the orientation of the electronic transition dipole moments (ETDM) of the first allowed electronic transition of the guests. The two types of molecules on the top left are small enough to fit into one unit cell of the host and their shape is such that the ETDM can be oriented perpendicular or nearly perpendicular to the channel axis. The next molecule needs more space and is tilted by an angle of about 45°. The molecules in the middle and on the right side are so large and of such a shape that only parallel or nearly parallel orientation with respect to the channel axis is possible. We illustrate in Figure 1(B,B') assemblies of molecules which align their ETDM parallel and perpendicular to the channel axis and which have no interaction because their shape keeps them at sufficiently large distance. But they are close enough, so that efficient Förster resonance energy transfer (FRET) can take place. Orientation of large molecules which align their ETDM parallel and perpendicular to the channel axis is also shown in Figure 1(C,C'). The shape of these molecules still does not allow orbital overlap but the distance is short enough so that important Davydov coupling[18] occurs, leading to exciton states.

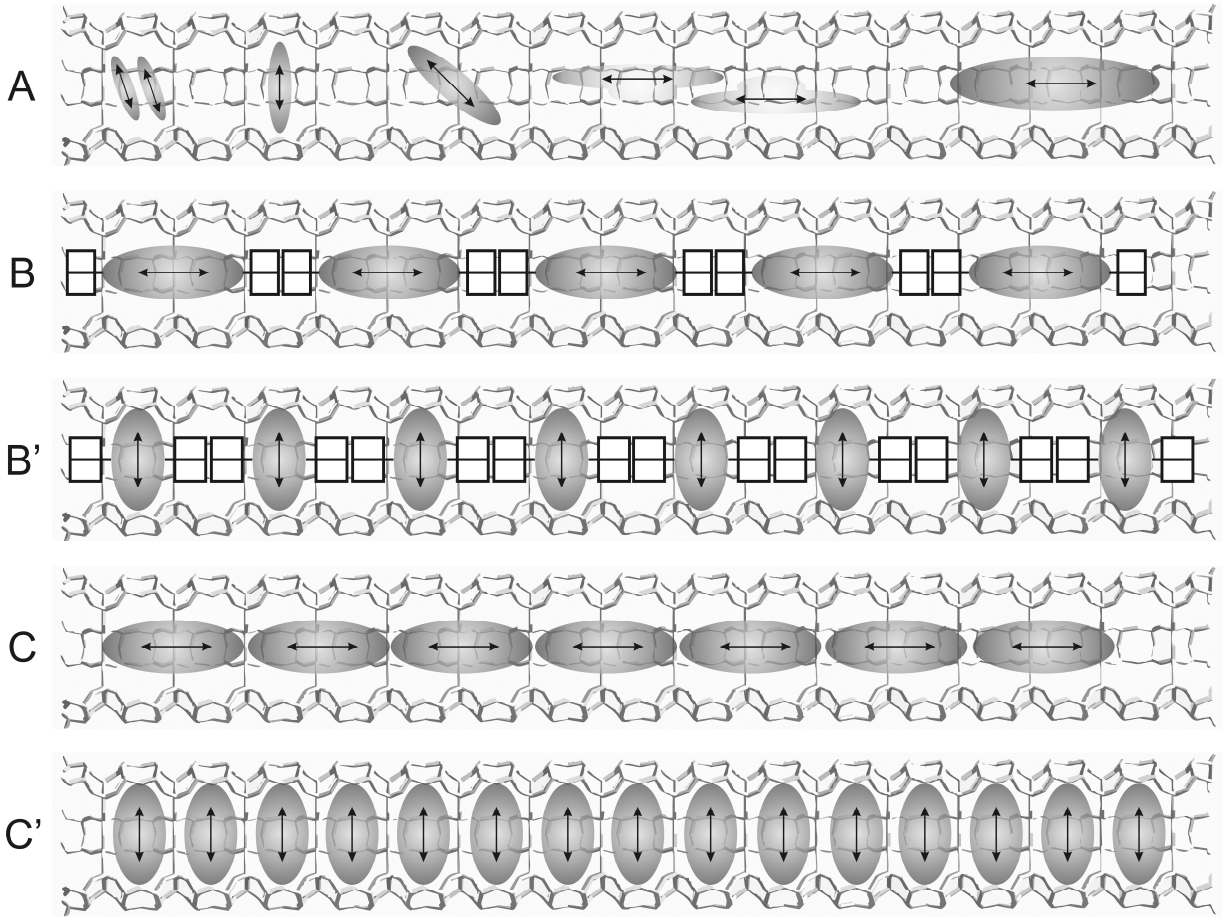

Figure 1. Different orientations and two arrangements of molecules in 1D channels. (A) Four representative orientations of molecules with different packing. (B) Orientation of molecules which align their ETDM parallel and (B') perpendicular to the channel axis and which have no interaction because their shape keeps them at sufficiently large distance. (C) Orientation of large molecules which align their ETDM parallel and (C') perpendicular to the channel axis and which are so close that Davydov coupling is important.

ZL has been found to be a very useful 1D channel host for synthesizing a large variety of host-guest composites with interesting photochemical and photophysical properties. The orientation and interaction of the dyes inside of the 1D channels have been studied experimentally. Dye-ZL composites with efficient FRET and impressive antenna properties have been synthesized and therefore considered for designing dye-nanochannel hybrid materials for light harvesting, transport and trapping.[3,5,15] Several composites where important Davydov coupling between dyes located in the channels occurs have been reported recently.[15,17,19-21] Understanding the packing of the dyes and their orientation inside of the channels is very important for understanding these dye-ZL composites and for learning how their properties can be influenced by e.g. molecular

engineering. The structure of methylviologen-ZL has been studied by means of powder X-ray and vibrational spectroscopy.[22] Most studies, however, rely on powerful optical microscopy investigations of single crystals in the size range of half a micrometer up to several micrometers.[15,19,20,23-26] These methods are related to the orientation of the ETDM of the first allowed electronic transition of the molecules. This molecular property is usually well known as it can be measured by several methods and often also accurately calculated with moderate computational effort. A cone angle type distribution was found to be a useful description of the room temperature equilibrium arrangement of the guest inside the 1D channels of ZL.[23] We show in Figure 2 optical fluorescence microscopy images of three cases: the acridine dye MeAcr is of a size and shape such that it fits into one unit cell of ZL and aligns perpendicular to the channel axis, while the perylene dye PR149 is so long that it occupies about 3 unit cells and has therefore no other option than to align parallel to the channel axis. The situation is more complex for the cationic molecules pyronine (Py^+) and oxonine (Ox^+) which are of nearly the same size and which can be inserted into the channels of ZL by means of cation exchange. Detailed optical microscopy studies of Py^+ and of Ox^+ loaded ZL were performed and cone angles with respect to the channel axis of more than 70° have been reported for both.[23,24] Similar results were found in angle-dependent fluorescence measurements of monolayers of oriented dye-zeolite L crystals.[15] The measurements were performed under ambient conditions and therefore refer to hydrated samples. All experimental methods used for these measurements average over a large number of channels and molecules. The number of channels n_{ch} of a crystal of diameter d_{ZL} expressed in nanometers can be estimated as follows:

$$n_{ch} = 0.267(d_{ZL})^2 \quad (1)$$

This means that a ZL crystal of 1 micrometer diameter consists of roughly 2.6×10^6 strictly parallel channels.[27,28] Single molecule studies have been reported for $ALPO_4$-5 but seem to be more conclusive for the larger pore systems such as M41S.[29]

The result that the orientation of Ox^+ can be represented by a cone type distribution with a half-cone angle of about 72° was accepted but not understood because it was not compatible with simple geometrical reasoning as it has been discussed in ref. [23]. Measurements were therefore repeated and extended by polarimetric two-photon fluorescence microscopy with several dyes, among them Ox^+ and Py^+ which are of very similar size and shape. The results are similar as those reported earlier but it was concluded that a cone-bell-shaped distribution with angles Θ for the aperture and Ψ for the width is better suited for representing the observed disorder than a rigid cone model. The values reported are Θ = 77° and Ψ = 24° for Ox^+ and Θ = 80° and Ψ = 15° for Py^+, all values with margins of a few degrees.[24] Since these results are essentially the same, as those reported earlier for Ox^+ they pose the same problem for understanding them. We have therefore added a question mark for the value of the cone angle β in Figure 2 (B).

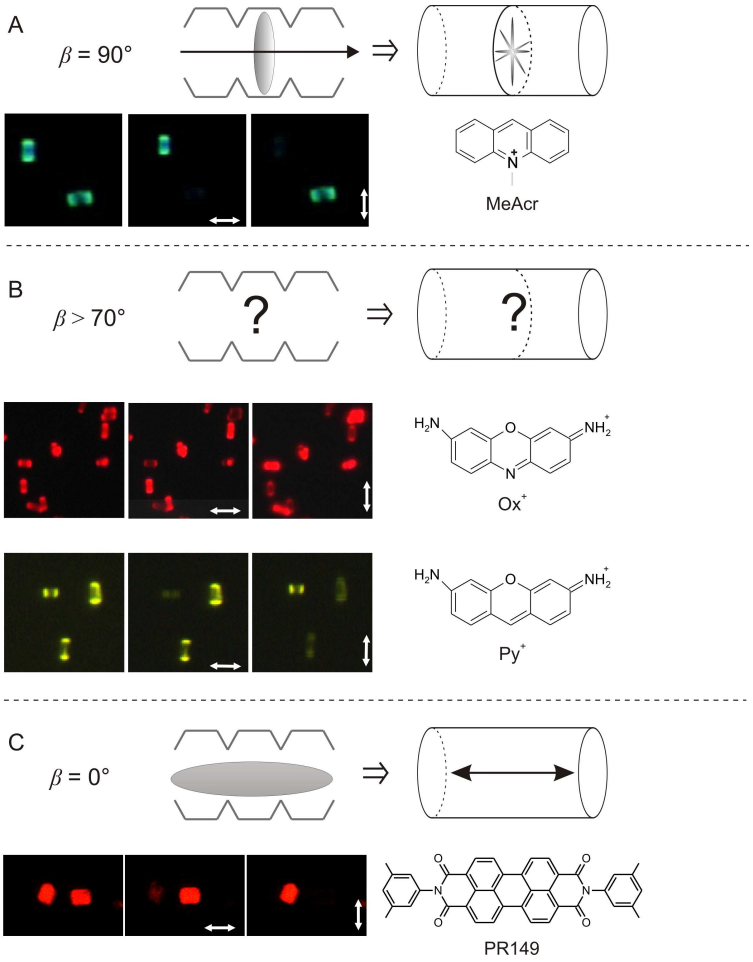

Figure 2. Fluorescence microscopy images of the orientation of dye molecules inside of a channel. (A) The orientation of the ETDM is perpendicular to the channel axis, β = 90° and therefore reduces to a plane. (B) The angle β of a cone shape angle distribution has been measured to be larger than 70° for both dyes. (C) The orientation is parallel to the channel axis, β = 0°. The double cone distribution reduces to a line.[15]

We have recently reported extensive first-principles investigations on the fluorescent dye fluorenone inside zeolite L, both at dry conditions and in the presence of water and we have succeeded to unravel the molecular origin of the peculiar stability of the fluorenone-ZL composite in humid environments. We also found that the cone angle distribution is a good way for describing the orientation of the dye.[30] Fluorenone is a dye which is smaller than MeAcr and bears therefore more flexibility for arranging inside of the ZL channels. Encouraged by these results we have decided to perform similar first-principles investigations regarding the equilibrium position of xantene dyes in ZL in order to comprehend fluorescence microscopy

results. These investigations led to a new insight and a different interpretation of the experimental observations which we report in this communication.

2. Computational Section

In view of the very similar structure and shape of the Ox^+ and Py^+ dyes, the theoretical investigation of xantene dye-ZL composites was carried out on Ox^+/ZL systems of different size and hydration degree and integrated by performing a selected set of calculations with Py^+ as a guest in the largest ZL models. Several simulation runs with different initial conditions (e.g. positioning/orientation of the dye, water molecules' arrangement) have been performed.

Oxonine-zeolite L (Ox^+/ZL) host-guest composites were studied by using the PBE approximation[31] to Density Functional Theory (DFT) and periodic boundary conditions. Models characterized by different size of the periodically repeated simulation cell were built and the all-potassium-form of ZL has been considered,[32a] in line with the composition of the samples adopted in the experiments of Ref. 23,24. The simulation cell of the smaller models (2c-models) contained two ZL unit cells along c (a=b=18.466 Å; c=2×7.476 Å; β=120°),[32a] corresponding to a framework formula of $[Al_{18}Si_{54}O_{144}]$, as Si and Al are in a 3:1 ratio in ZL. Since 18 monovalent extraframework cations are needed to balance the framework negative charge, the simulation cell formula is $K_{17}[Al_{18}Si_{54}O_{144}]Ox^+$. Ox^+/ZL models corresponding to dry and hydrated hybrid composites were investigated by exploring both 0 K energy minima (geometry optimizations) and room temperature behaviour (first principles molecular dynamics simulations).

The simulation cell content of the dry system (2c-ZL/Ox^+) was $K_{17}[Al_{18}Si_{54}O_{144}]Ox^+$. In the case of the hydrated composite, the amount of water in the simulation cell was chosen on the basis of the available literature data on ZL and ZL-based composites. For the synthetic ZL without guests, the experimental water content per unit cell is 21 H_2O[32b] at room temperature and 98 % rel. humidity, but it drops to 16 H_2O per unit cell at room temperature and 22 % rel. humidity; i.e. close to the experimental conditions under which most results herein referred have been obtained. Moreover, as indicated by TGA and DTG measurements,[3c] as well as by X-ray structural analysis,[22] the ZL water content further drops if guests are inserted because they occupy space according to their van der Waals volume. As a consequence, the water content is much lower than in pristine Zeolite L, e.g., 12 H_2O and 8-10 H_2O per unit cell were reported for methylviologen-ZL[22] and for p-Terphenyl-ZL[3c] composites, respectively. The number of water molecules per unit cell corresponding to the experimental conditions at which the fluorescence microscopy experiments on Ox^+/ZL and Py^+/ZL were carried out can only be estimated to be in the range of about 9-12 water molecules per ZL unit cell. On these basis, calculations have been performed on a series of models characterized by different water contents within that range, i.e., 9, 10.7, and 12 water molecules/unit cell. Specifically, the 2c-hydrated system $K_{17}[Al_{18}Si_{54}O_{144}]Ox^+\bullet(H_2O)_{18}$ (2c-ZL/$Ox^+\bullet 18H_2O$) was modeled with a water content of $9H_2O$ per cell, compatible with what expected for a zeolite L containing one Ox^+ per two unit cells at

22 % rel. humidity, and both geometry optimizations and FPMD simulations were performed. Moreover, geometry optimization calculations were performed on a 2c-model of the composite containing 24 H_2O molecules, *i.e.*, 12 water molecules per unit cell ($K_{17}[Al_{18}Si_{54}O_{144}]Ox^+ \bullet (H_2O)_{24}$, 2c-ZL/$Ox^+ \bullet 24H_2O$).

The initial water positions were chosen from the crystallographic water oxygen sites of the pristine fully hydrated ZL[32b], which have fractional occupancy (0.2 to 0.7). More specifically, the guess configuration for a given positioning/orientation of the dye and water loading was designed by eliminating water molecules in closest contact with the organic dye. Different initial choices of water positions have been considered as well. For instance, the water sites reported for the methylviologen-ZL composite[22] were also taken into account, and in the case of the 2c-ZL/$Ox^+ \bullet 18H_2O$ model with perpendicular Ox^+ two alternative guesses were built. Such starting configurations, in which the O(7) and O(8) sites were occupied with 12 and 6 H_2O's, respectively and 10 and 8 H_2O's respectively, finally led to virtually identical optimized structures. In general, the choice of the water molecules' positioning in the guess configuration did not significantly affect equilibrium geometries/energy minima of the composite because during equilibration (or simulated annealing for geometry optimization) water molecules rearranged with respect to their initial locations.

Whereas in 2c-ZL/$Ox^+ \bullet 18H_2O$ the 18 water molecules were all placed inside the ZL channel, in the case of 2c-ZL/$Ox^+ \bullet 24H_2O$ 21 H_2Os were located in the channel and 3 in the ZL small cages.[3c]

The starting positioning of the dye molecule in the FPMD runs was chosen in such a way to obtain a specific initial orientation with respect to the channel axis. Several sets of initial positions were tested, in particular coordinates corresponding to molecular orientations α of approximately 0°, 70° and 90° were considered. Local energy minima were mainly obtained starting from configurations extracted from the FPMD trajectories, even though in some cases starting guesses characterized by a specific desired initial orientation of the dye were built. For each calculation presented in this work, the initial orientation of the dye with respect to the ZL channel axis is reported in Tables 1-4.

All of the 2c systems are characterized by a concentration of 0.5 Ox^+ molecules *per* unit cell (experimental data refer to 0.0003 in ref [23] and between 0.005 and 0.025 in ref [24], dye molecules *per* cell).[23,24] Larger model systems (3c-models), containing three ZL cells along c (a=b=18.466 Å; c=3×7.476 Å; β=120°) and corresponding to a concentration of 0.3 Ox^+ *per* unit cell were considered as well, both in the dry ($K_{26}[Al_{27}Si_{81}O_{216}]Ox^+$ (3c-ZL/Ox^+)) and in the hydrated ($K_{26}[Al_{27}Si_{81}O_{216}]Ox^+ \bullet (H_2O)_{32}$ (3c-ZL/$Ox^+ \bullet 32H_2O$)) forms. The water content of the hydrated 3c-model corresponds to 10.7 H_2O molecules per unit cell, and all of the 32 H_2Os were located inside the ZL channel.

In all simulations, electron-ion cores interactions were described with ultra-soft Vanderbilt pseudopotentials for H, C, O; norm conserving pseudopotentials for Si, Al, K (semi-core).[33] Electronic orbitals were expanded in planewaves up to a 25 Ry cutoff (200 Ry for the density).

This electronic structure calculation scheme provides a good description of large sized inorganic-organic systems including dye-zeolite hybrids.[30,34]

First principles molecular dynamics (FPMD)[35] simulations on all the Ox^+/ZL models were run with a time step of 0.121 fs and an inertia parameter of 500 au for the electronic states coefficients. After equilibration, trajectories were collected for ~12 ps and ~4 ps for the 2-cells and 3-cells models, respectively (simulation lengths reported in Table 4). Simulations were performed in the canonical ensemble (target temperature of the ionic thermostats: 300 K). Minimum energy structures of Py^+ encapsulated in ZL were calculated on dry and wet 3c models ($K_{26}[Al_{27}Si_{81}O_{216}]Py^+$ (3c-ZL/Py^+) and $K_{26}[Al_{27}Si_{81}O_{216}]Py^+ \bullet (H_2O)_{32}$ (3c-ZL/$Py^+ \bullet 32\ H_2O$), respectively). In this case, the optimized structures obtained for the corresponding 3c-models containing Ox^+ were chosen as starting geometries and the central Ox^+ nitrogen was replaced by a C-H group. Such guess configurations were used as input for the simulated annealing/geometry optimization cycles.

Local energy minima were generally obtained by performing simulated annealing/geometry optimization cycles on selected configurations extracted from the simulations. Geometry optimizations were performed by quasi-Newton methods (convergence criterion: maximum force on nuclei of 1×10^{-4} hartree/bohr). In all optimizations and molecular dynamics simulations, all atoms were allowed to move, no symmetry constraint (except from the box shape and size) was imposed, and periodic boundary conditions were applied.

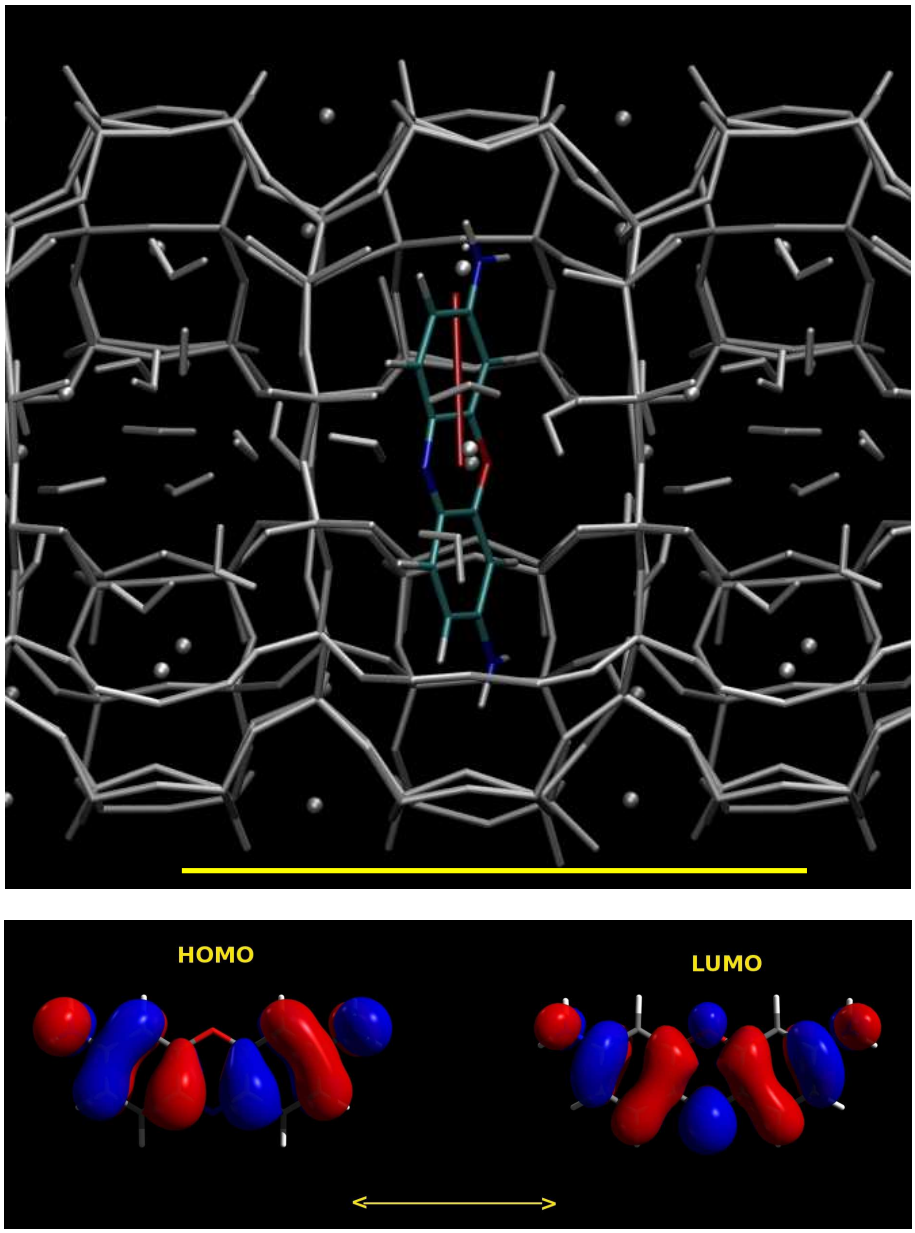

Figure 3. Top panel: graphical representation of the minimum energy structure of the hydrated 2c-ZL/Ox^+•$18H_2O$ system evidencing the alignment of the Ox^+ calculated ETDM (red vertical bar) with the Ox^+ molecular axis. α and β are defined, respectively, as the angles formed by the molecular axis and by the ETDM with the channel axis. O: red; N: blue; C: cyan; H: white. ZL framework atoms, K^+ cations and water molecules are represented in gray. The yellow line indicates the simulation cell dimension (periodicity) along the channel direction. Bottom panel: Ox^+ HOMO and LUMO, involved in the first Ox^+ excitation, and the corresponding ETDM orientation (yellow arrow).

Calculations of the first excited singlet state (S_1) of hydrated Ox^+/ZL were carried out by using a restricted open-shell Kohn-Sham Hamiltonian within the low-spin-excitation (LSE) formalism.[36] Such an approach can deal with low-spin excited states of both molecular and condensed phase systems, in particular it has been successfully applied to the study of electronic excitation transfer events in zeolites with one-dimensional channel systems.[37] LSE calculations were performed on the periodic 2-cell model system 2c-ZL/Ox^+•$18H_2O$ starting from the ground-state (S_0) minimum energy structure. Such an S_0 geometry was first reoptimized by using norm-conserving pseudopotentials (NCPP) [33b-d] for all atoms and a cutoff of 80 Ry, obtaining essentially identical results; then, a geometry optimization in S_1 was carried out, with LSE, NCPP and a 80 Ry cutoff.

Calculations of the electronic transition dipole moment (ETDM) were performed on the Ox^+ molecule $(C_{12}H_{10}ON_3)^+$ and on $Ox^+(H_2O)_n$ subsystems extracted from FPMD configurations/optimized structures of the Ox^+/ZL models with the Gaussian09 code.[38] Other test calculations were performed on Ox^+ systems characterized by asymmetric and/or charged environments, e.g. hydrated Ox^+, hydrated Ox^+-Cl^-. (see Supporting Information). Optimizations of the isolated complexes $Ox^+ \cdot H_2O$ and $Py^+ \cdot H_2O$ were performed at the MP2/cc-pvtz level of theory.[38]

3. Results

The orientation and positioning of Ox^+ in the ZL nanochannels were investigated on Ox^+/ZL model systems characterized by different initial orientations of the molecule, both at dry conditions and in the presence of water. In order to compare our results with the orientation deduced from optical experiments of hydrated samples, we first verified whether the orientation of the Ox^+ electronic transition dipole moment could actually be approximated by the long molecular axis. The first electronic excitation was calculated for different Ox^+ configurations, obtaining in all cases very small deviations of the ETDM from the Ox^+ axis (< 5º) even in the presence of anisotropic environments or deformed Ox^+ geometries (see Supporting Information). In the case of the minimum energy structures such a deviation is negligible, as clearly shown in Figure 3. On this basis, in Ox^+/ZL the ETDM can be considered aligned with the Ox^+ axis and the angle α, calculated from geometric parameters obtained from the simulations, can be safely compared with the half-cone angles β deduced from optical measurements.

The orientation of the molecule in the optimized structures of the Ox^+/ZL models, its distortion from planarity and hydrogen bond interactions, as well as the relative stability of energy minima calculated for both dry and wet conditions are collected in Tables 1 and 2, respectively. Remarkably, the energetically favoured Ox^+ orientation radically changes when passing from the dry to the hydrated composite, pointing to a key role of water in governing the dye orientation in

Ox^+/ZL composites. As clearly shown by the minimum energy structures of the larger model systems in Figure 4, the molecule is approximately aligned to the ZL channel axis at dry conditions, but becomes perpendicular in the hydrated model. In particular, in the former case (Fig 4a), Ox^+ is oriented at α=14.0º and is positioned close to the ZL channels' walls forming two weak hydrogen bonds with framework oxygens. In such an arrangement, the molecule occupies two unit cells of the host. On the other hand, at wet conditions (Fig. 4b) Ox^+ is caged into one single ZL unit cell, hydrogen bonded with its NH_2 groups to framework oxygens on opposite sides of the cavity and oriented at α=88.1º. The N atom in the Ox^+ central ring is strongly involved in the water hydrogen bonded network, which extends throughout the ZL channel and to potassium counterions and framework oxygens as well. Interestingly, only few water molecules are relatively close to Ox^+. Indeed, the water subsystem is mainly clustered in the adjacent, dye-free ZL unit cells in a quasi-tetrahedral organization quite common in zeolites, closely resembling that of water in the condensed phases.[3c,39] Even more significantly, the water oxygens are located quite close to the water crystallographic positions determined by diffraction for the all-potassium natural counterpart of ZL, i.e. the zeolite perlialite.[32c]

It should also be noticed that, even though the most stable structures of dry- and hydrated-Ox^+/ZL are characterized by different Ox^+ orientation, positioning and interactions, Ox^+ maintains the planar molecular geometry pertaining to the isolated, gas phase molecule independently of the water content. Similar results are found for the smaller models as well, indicating that the simulation system size has only minor effects on the minimum energy structures, in particular it does not affect the orientation and the geometry of the molecule.

In order to check whether electronic excitation would induce deformation of the Ox^+ structure or changes of its orientation, we modelled, on the minimum energy structure of the hydrated 2c-ZL/Ox^+•$18H_2O$ model Opt1, a photoexcitation process via a Hamiltonian switch from the ground to the first excited singlet state. More specifically, while the ground-state of the system was described by the standard Kohn-Sham Hamiltonian, the first excited singlet system was modelled by using a restricted open-shell Kohn-Sham Hamiltonian within the LSE approach,[36] and its geometry optimized. The resulting S_1 minimum energy structure, Opt1*, is very similar to Opt1. This result indicates that electronic excitation does not cause significant distortion of the molecular geometry and does not alter Ox^+ orientation; on the macroscopic scale, this means that absorption and emission optical data should provide the same information on Ox^+ orientation. This result is in full agreement with the mirror symmetry between the absorption and fluorescence spectra observed for this dye in solution and in ZL.[23,28]

System	α_{start}	α	δ[a]	Ox^+/O_{frame} HB	ΔE (kcal/mol)
2c-ZL/Ox^+					
Opt1	13.3	15.6	177.9	2.041 2.043	0
Opt2	10.3	7.25	165.5	2.061 2.119	2.31
Opt3	87.5	89.7	171.5	2.058 2.125 2.112 2.155	3.83
Opt4	48.7	51.4	179.9	1.848 1.866 2.272 2.273	16.2
3c-ZL/Ox^+					
Opt1	15.6	14.0	176.2	1.976 2.047	0
Opt2	89.7	89.5	171.3	2.060 2.120 2.151 2.155	18.9

Table 1. Optimized structures for dry Ox^+/ZL with different Ox^+ orientation α. Ox^+ orientation in the starting configuration α_{start}, Ox^+ torsion angles δ, hydrogen bond distances (HB) and energy differences ΔE with respect to the minimum energy structure (ΔE=0) are also reported for each simulation system. Angles in degrees, distances in Å, energies in kcal/mol. Minimum energy structures highlighted in bold.

[a]The torsion angle δ is defined as the dihedral formed by the Ox^+ atoms (H_2)N-O-N-N(H_2)

System	α_{start}	α	δ [a]	Ox^+/O_{frame} HB	Ox^+/H_2O HB	ΔE (kcal/mol)
2c-ZL/Ox^+•18H_2O (9 H_2O per u.c.)						
Opt1	86.2	89.2	179.5	1.815 1.960 1.859 2.116	1.778 (N_{Ox}-H_w)	0
Opt1* [b]	89.2	89.4	178.5	1.789 1.968 1.836 2.118	1.704 (N_{Ox}-H_w)	-

Opt2	1.9	7.9	176.3	2.309	1.834 (N_{Ox}-H_w) 1.944 (H_{Ox}-O_w) 2.225 (H_{Ox}-O_w)	6.72
Opt3	44.2	45.2	170.8	1.748	1.718 (N_{Ox}-H_w) 2.070 (H_{Ox}-O_w) 2.157 (H_{Ox}-O_w)	8.43
Opt4	15.6	18.7	164.0	2.135 2.194	1.896 (N_{Ox}-H_w) 1.994 (N_{Ox}-H_w) 1.978 (H_{Ox}-O_w) 2.100 (H_{Ox}-O_w)	10.34
Opt5 [c]	74.4	88.7	179.4	1.859 1.947 1.833 2.221	1.856 (N_{Ox}-H_w)	1.04
Opt6 [d]	69.4	50.4	168.2	1.799	1.884 (N_{Ox}-H_w) 2.138 (H_{Ox}-O_w) 2.166 (H_{Ox}-O_w)	10.45
2c-ZL/Ox^+•24H_2O (12 H_2O per u.c.)						
Opt1	72.0	88.8	175.1	1.933 1.965 1.896 2.210	1.797(N_{Ox}-H_w)	0
Opt2	18.0	25.0	173.4	2.055	1.866(N_{Ox}-H_w) 1.971(H_{Ox}-O_w) 2.234(H_{Ox}-O_w)	7.30
3c-ZL/Ox^+•32H_2O (10.7 H_2O per u.c.)						
Opt1	86.6	88.1	179.7	1.939 1.950	1.744 (N_{Ox}-H_w)	0
Opt2	19.6	20.4	169.7	1.928	1.799 (N_{Ox}-H_w) 1.884 (H_{Ox}-O_w) 2.055 (H_{Ox}-O_w)	3.26
Opt3	42.4	41.0	169.1	1.895 2.280	1.752 (N_{Ox}-H_w) 1.919 (H_{Ox}-O_w) 1.971(H_{Ox}-O_w)	7.00

Table 2. Optimized structures for hydrated Ox^+/ZL with different Ox^+ orientation α. Ox^+ orientation in the starting configuration α_{start}, torsion angles δ, hydrogen bond distances (HB) and energy differences ΔE with respect to the minimum energy structure (ΔE=0) are also reported for each simulation system. Angles in degrees, distances in Å, energies in kcal/mol. Minimum energy structures highlighted in bold. [a]The torsion angle δ is defined as the dihedral formed by the Ox^+ atoms (H_2)N-O-N-N(H_2). [b]Opt1* is the optimized geometry of the first excited singlet state for the 2-cell model. [c]See also Movie 3 in the Supporting information. [d]See also Movie 4 in the Supporting information.

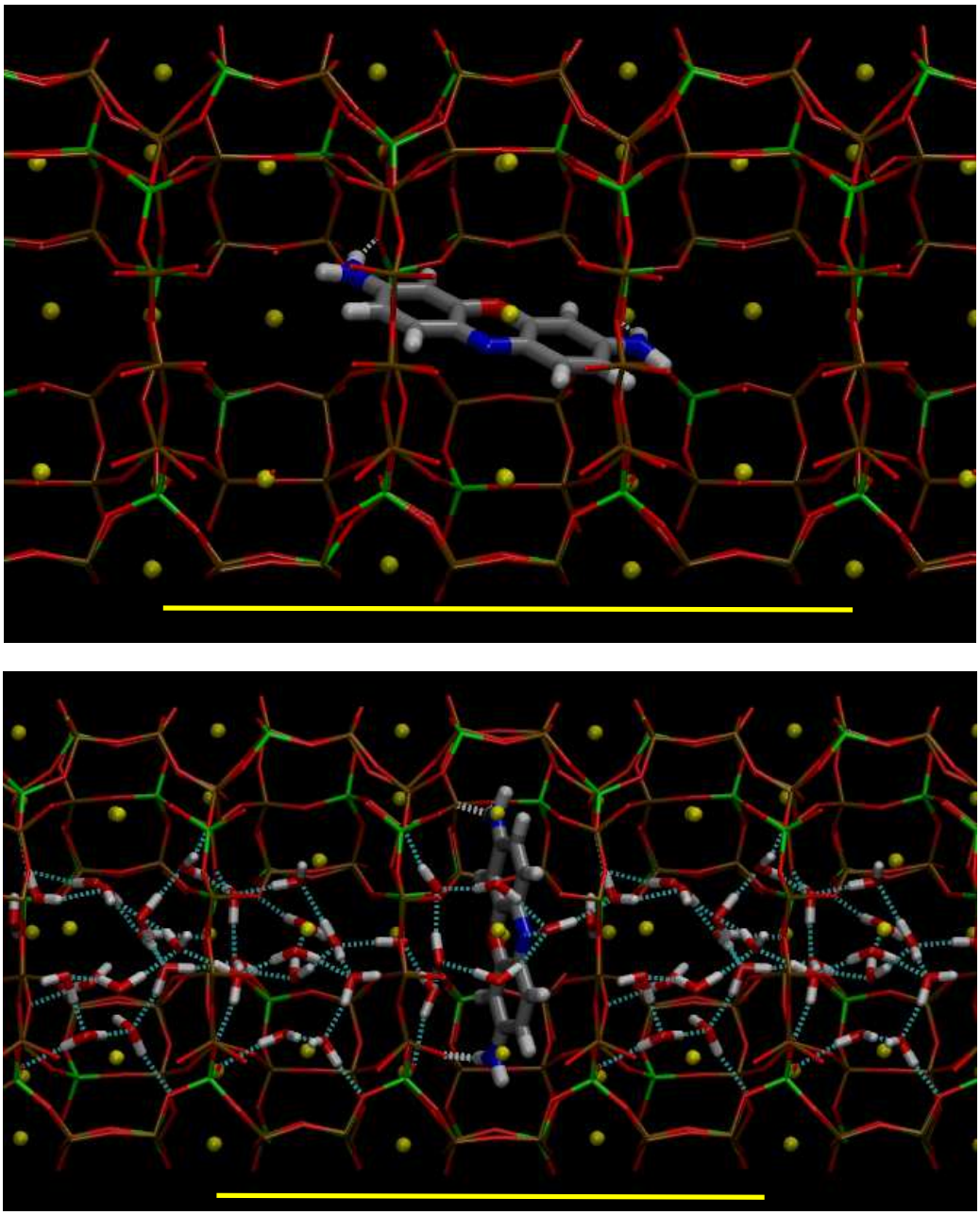

Figure 4. Minimum energy structures for the Ox^+/ZL 3-cell models. Top panel: dry Ox^+/ZL system, 3c-ZL/Ox^+, Opt1 (see Table 1). Bottom panel: hydrated Ox^+/ZL system, 3c-ZL/Ox^+•$32H_2O$, Opt1 (see Table 2). Color codes: Al: green, Si: brown, O: red, K: yellow, N: blue, C: gray, H: white. Cyan dotted lines represent hydrogen bonds involving water molecules; hydrogen bonds between Ox^+ and ZL framework oxygens are represented as thick white dotted lines. The yellow line indicates the simulation cell dimension (periodicity) along the channel direction.

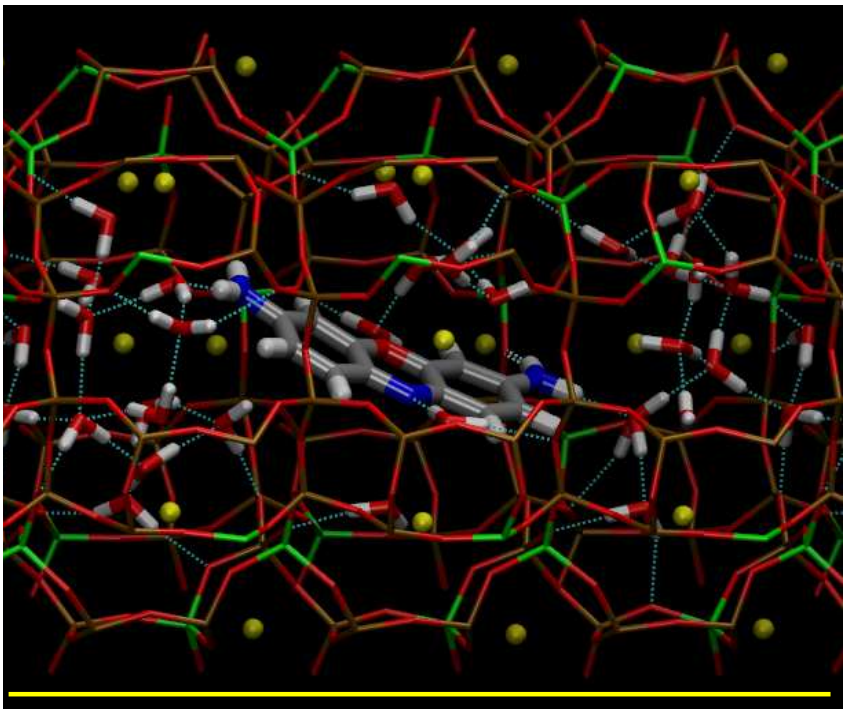

Figure 5. Optimized structure Opt2 for the hydrated Ox^+/ZL system (32 H_2O) with α=20.4º (Table 2). Color codes: Al: green, Si: brown, O: red, K: yellow, N: blue, C: gray, H: white. Cyan dotted lines represent hydrogen bonds involving water molecules; hydrogen bonds between Ox^+ and ZL framework oxygens are represented as thick white dotted lines. The yellow bar marks the periodicity along the channel direction.

Data in Tables 1-2 also suggest that other arrangements, characterized by Ox^+ orientation different from the minimum energy ones, may be possible for the Ox^+/ZL system, both at dry and wet conditions. In the case of the hydrated composite, for both 3-cell and 2-cell models we obtained optimized structures in which Ox^+ is approximately aligned parallel to the channel, as shown in Figure 5 for the 3-cell system. Here, Ox^+ occupies two ZL cells, is slightly distorted from planarity and interacts with both water molecules and AlO_4 framework oxygens, via three strong hydrogen bonds in the former case and a weaker one in the latter (see also Table 2). This Ox^+/ZL geometry is 3.26 kcal/mol higher than the minimum energy structure and is therefore thermally accessible to the system at room conditions, suggesting that, in the presence of water, Ox^+ is preferentially perpendicularly oriented but it might also be found roughly parallel. Besides these extreme orientations, optimized geometries with Ox^+ at α=40÷50º with respect to the channel axis were also found, at a slightly higher energy. Nevertheless, none of the calculated structures featured Ox^+ with α in the 70-85º range. Such a finding holds also for the dry system,

for which optimized structures (at higher energy) with α either ~90º or in the 40÷53º range were obtained only.

Table 3 reports the main features of the Py^+-ZL composite. In the predicted minimum energy structure of the hydrated system (3c-ZL/Py^+•$32H_2O$), Py^+ is oriented with α=87.9° (figure 6a). This geometry is 4.86 kcal mol^{-1} more stable than the structure characterized by an α value of 18.1°. For the anhydrous (3c-ZL/Py^+) model, the structure with α=13.6° is more stable with respect to the structure characterized by α = 89.8° by 19.50 kcal mol^{-1}(figure 6b). In both cases, the predicted most favourable Py^+ orientation, as well as the energy differences between alternative Py^+ orientations, are very close to those found for $Ox^{\pm}$, and, remarkably, no stable structure with α in the 70-85º range has been found. In addition, as evidenced by Figure 6, even very subtle details of the Py^+ arrangement inside ZL are strikingly similar to the Ox^+ case. In the hydrated composite, Py^+ NH_2 groups form strong hydrogen bonds with framework oxygens on opposite sides of the channel in one ZL unit cell, and the CH group proton of the central Py^+ ring is at 2.092 Å distance from a water oxygen involved in the water hydrogen bonding network. Indeed, such a proton can be engaged in hydrogen bonding with a water molecule: the resulting structure is very similar to that of Ox^+ hydrogen bonded to a water proton via the central nitrogen atom, as shown by the optimized structures of the Py^+•H_2O and Ox^+•H_2O complexes in the vacuum (see Figure 6, bottom). The Py^+•H_2O $H^{\cdots}O_{water}$ and Ox^+•H_2O $N^{\cdots}H_{water}$ distances (2.118 and 1.984 Å, respectively), as well as the $C^{\cdots}O_{water}$ and $N^{\cdots}O_{water}$ distances (3.203 and 2.941 Å, respectively), indicate a very close spatial arrangement, with a slightly weaker hydrogen bond in the case of Py^+. These results rationalize all experimental evidences[5] showing a very similar behavior for Py^+ and Ox^+ in zeolite L.

System	α_{start} (º)	α (º)	δ(º)[a]	Py^+/O_{frame} HB	Py^+/H_2O HB	ΔE (kcal/mol)
3c-ZL/Py^+						
Opt1	14.0	13.6	176.5	1.969 2.013	-	0
Opt2	89.5	89.8	175.5	2.100 2.118 2.143	-	19.50
3c-ZL/Py^+•$32H_2O$ (10.7 H_2O per u.c.)						
Opt1	88.1	87.9	179.9	1.945 2.002 2.007	2.092 (CH_{Py}-O_w)[b]	0
Opt2	20.4	18.1	171.3	2.013	1.919 (NH_{2Py}-O_w)	4.86

Table 3. Optimized structures for dry and hydrated Py^+/ZL 3c-models with different Py^+ orientation α. Py^+ orientation in the starting geometry α_{start}, torsion angles δ, hydrogen bond distances (HB) and energy differences ΔE with respect to the minimum energy structure (ΔE=0) are also reported. Angles in degrees, distances in Å, energies

in kcal/mol. Minimum energy structures in bold. [a]The torsion angle δ is defined as the dihedral formed by the Py^+ atoms (H_2)N-C(H)-N-N(H_2). [b]Distance between the H atom of the CH group in the central Py^+ ring and water oxygen.

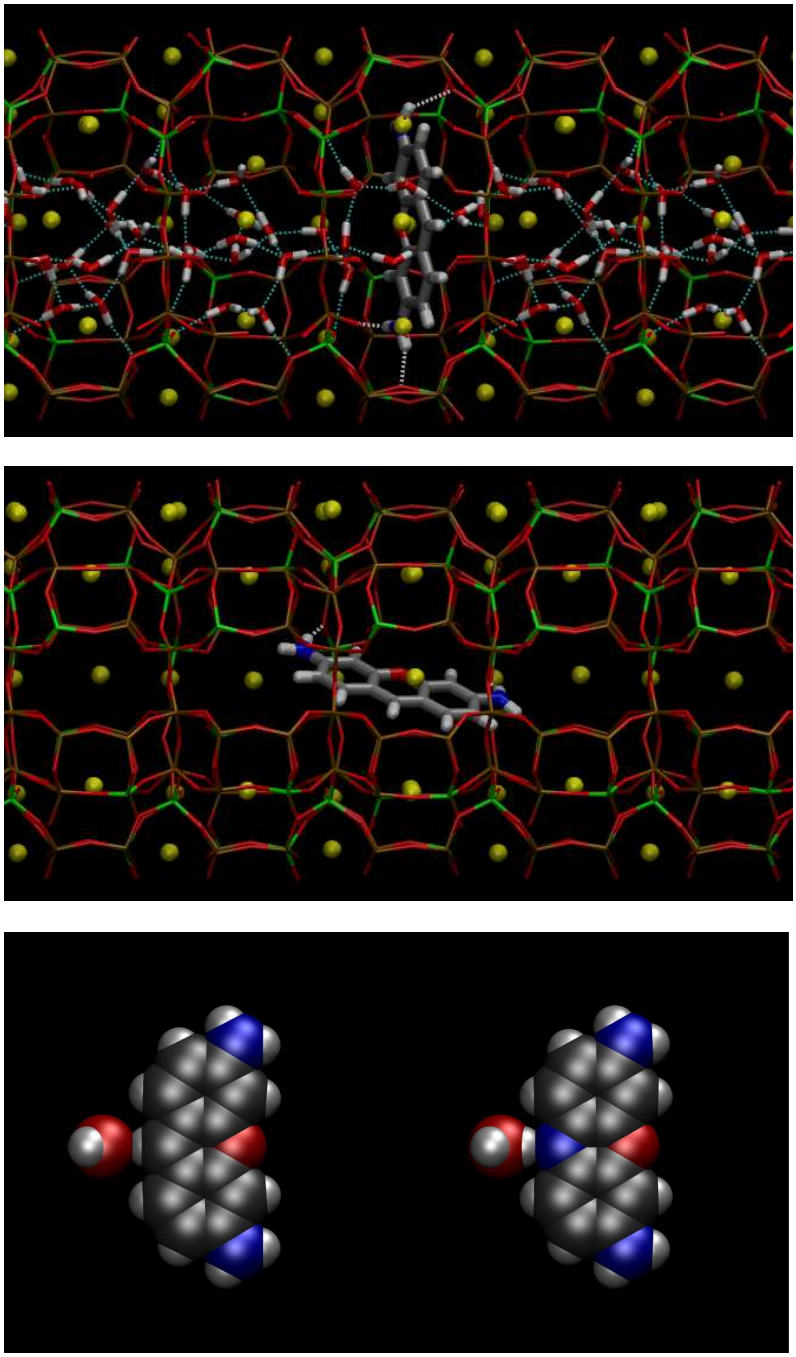

Figure 6. Top panel (a): Minimum energy structure of the hydrated Py^+/ZL 3-cell system, 3c-ZL/Py^+•32H_2O, Opt1 (see Table 3). Center panel (b): Minimum energy structure of the dry Py^+/ZL 3-cell

system, 3c-ZL/ Py^+, Opt1 (see Table 3). Bottom panel (c): Minimum energy structures of the isolated complexes $Py^+ \bullet H_2O$ (left) and $Ox^+ \bullet H_2O$ (right). Color codes: Al: green, Si: brown, O: red, K: yellow, N: blue, C: gray, H: white. Cyan dotted lines represent hydrogen bonds involving water molecules; hydrogen bonds between Ox^+ and ZL framework oxygens are represented as thick white dotted lines.

System	Time	α_{start}	α_{ave}	α_{min}	α_{max}	δ_{ave}	δ_{min}	δ_{max}
2c-ZL/Ox^+								
D1	11.5	7.2	20.3 (7.1)	5.5	40.2	168.5 (8.1)	143.9	180.0
D2	11.6	88.1	87.3 (2.0)	79.2	90.0	171.7 (5.9)	156.1	180.0
D3	6.7	51.4	38.5 (11.9)	13.2	64.4	170.4 (6.9)	150.1	180.0
D4 [a]	12.1	89.2	19.5 (14.5)	0.8	89.2	164.0 (19.2)	78.0	180.0
3c-ZL/Ox^+								
D5	4.1	89.2	88.2 (1.3)	84.2	90.0	167.6 (10.2)	140.2	180.0
2c-ZL/$Ox^+ \bullet 18H_2O$								
W1	14.2	84.7	87.4 (1.9)	80.4	90.0	174.0 (4.4)	161.7	180.0
W2 [b]	21.4	56.4	45.1 (4.0)	34.0	57.8	171.7 (5.8)	151.5	180.0
W3	3.4	51.4	52.7 (5.7)	40.1	69.4	166.4 (9.1)	147.4	180.0
W4	7.3	18.7	8.3 (5.6)	0.1	25.3	172.2 (7.2)	138.2	180.0
3c-ZL/$Ox^+ \bullet 32H_2O$								
W5	4.2	88.7	87.1 (2.2)	79.3	90.0	173.1 (4.8)	161.1	180.0
W6	4.1	45.2	35.9 (6.2)	26.7	54.1	169.3 (9.9)	136.6	180.0
W7	4.1	18.7	20.5 (4.2)	5.8	28.6	166.2 (7.3)	147.0	180.0

Table 4. Ox^+ orientation α and Ox^+ torsion angles δ from MD simulations. Standard deviations (in parentheses) provide an estimate of average thermal fluctuations. The simulation length (ps), the maximum oscillations of α and δ and the orientation of the starting MD configuration are also reported. Angles in degrees (º). [a] See also Movie 1 in the Supporting Information. [a]See also Movie 2 in the Supporting Information.

The room temperature behaviour of the Ox^+/ZL composite is summarized in Table 4. Interestingly, a very different behaviour of the dye was observed at dry conditions by starting with Ox^+ either aligned or perpendicular to the channel axis (D1 and D2, respectively). Whereas in the former case Ox^+ moves back and forth along the channel, in the latter it always stays inside one single ZL unit cell, with both -NH_2 groups engaged in hydrogen bonds with AlO_4 framework oxygens. Moreover, the Ox^+ motion in D1 is accompanied by frequent changes of orientation, while the molecule remains roughly perpendicular to the channel axis in D2, where it appears to be locked up, even though this is not the most stable orientation at dry conditions. These different behaviours are highlighted by the corresponding α distributions, shown in Figure 7, whereas a broad distribution centred at 20.3º is collected for D1, a narrow peak averaging to 87.3º is obtained for D2. Since similar trends are also found for the x and y angles distributions (not shown), it may be concluded that, in the dry Ox^+/ZL composite at room conditions, if Ox^+ is

aligned to the ZL channel its motion is characterized by significant translational and orientational mobility with respect to both channel's axis and section, with large room temperature fluctuations from the minimum energy orientation. Otherwise, if Ox^+ is at α ~90º, it could stay encapsulated into one single ZL unit cell and maintain such a metastable orientation, even without rotating around its axis, as also confirmed by simulations performed on the larger model system (see Table 4 and Figure 7). Interestingly, temperature-induced fluctuations of the Ox^+ geometry from planarity also occur, and are more pronounced when the molecule orientation is different from the perpendicular one, as indicated by the average molecular torsion angle δ, its standard deviation and its maximum oscillation (Table 4).

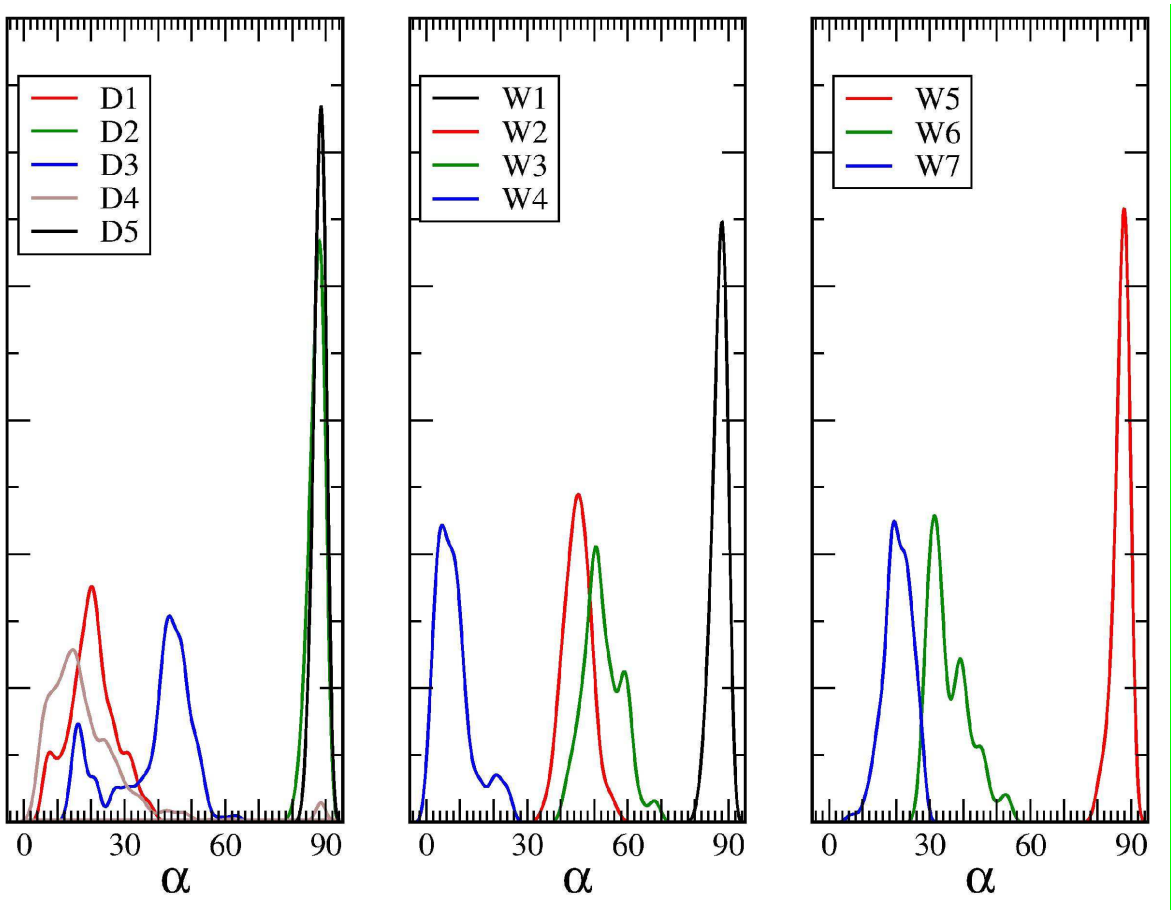

Figure 7. Distribution of the angle α for the dry Ox^+/ZL systems, for the hydrated models 2c ZL/Ox^+•18H_2O and for the hydrated models 3c ZL/Ox^+•32H_2O.

It would be now interesting to investigate the finite temperature behaviour of Ox^+ if its orientation is in between the aligned and the perpendicular ones. In simulation D3, starting from α =51.4º, Ox^+ recovers its minimum-energy orientation, roughly parallel to the channel, after a 6 ps equilibration period and then it behaves like in D1, i.e., with great translational and

orientational mobility as evidenced by the corresponding α distribution, characterized by a maximum at 45º and a growing peak at 12º related to Ox^+ reorientation. This result leads to the question: how could Ox^+ escape from the perpendicular arrangement, where it appears to be locked up, and recover its minimum energy orientation in the anhydrous composite. By keeping into account that Ox^+ is a charged molecule, reorientation might reasonably be induced, or at least influenced, by changes in the electrostatic potential of the host. To explore this possibility, we modelled in simulation D4 a charge unbalance by displacing one of the K^+ from the ZL unit cell occupied by a perpendicularly oriented Ox^+ to the adjacent cell. As an effect, the Ox^+ molecule bents so as to allow its escape from the cage and its entrance to an adjacent one, followed by fast motion along the channel direction (see Movie 1 in the Supporting Information). At equilibrium, Ox^+ recovers into the aligned orientation and shows the pertaining dynamical behaviour, as indicated by the α distribution (Figure 7) and the corresponding data in Table 4.

Also the finite temperature behaviour of the hydrated Ox^+/ZL composite is different from that of the dry system, as expected on the basis of the minimum energy structures results. Ox^+ shows, in general, a very low mobility and tends to maintain approximately its initial orientation, as indicated by data in table 4. Not surprising, oscillations of the Ox^+ positioning and orientation are smallest in the case of the perpendicular position (W1), however, no translation or drastic changes of orientation were detected, independently on model size or starting orientation. This behaviour is sketched, e.g. in Movie 2 (Supporting Information), representing a portion of the W2 trajectory, with α averaging to 45º. It can be easily seen that, due to the formation of strong hydrogen bonds with water, Ox^+ tends to maintain this orientation, which was not stable at room temperature conditions in the dry system (e.g. simulation D3). We recall that water forms a hydrogen bonded network inside the ZL channels, which involves zeolite framework oxygens and extraframework species as well. Previous work on zeolitic water[40-46] demonstrated that at these conditions the dynamic properties of water are dominated by hydrogen bonding, which implies a slowing-down of the water orientational dynamics in zeolite nanochannels, that in turn affects the motion of the dye. Therefore, the lower mobility and slower reorientation of Ox^+ with respect to the anhydrous system are due to the hampering effect of the water hydrogen bond network, an effect already detected and understood in the case of the Fluorenone/ZL composite.[30] The α distributions of the wet systems, also represented in Figure 7, are narrower than in dry conditions, as a consequence.

In spite of these differences in the Ox^+ orientational dynamics, the room temperature behaviours of the dry and the hydrated composite share two relevant common features: the presence of fluctuations from planarity of the Ox^+ molecular geometry, and the absence of stable Ox^+ arrangements with α in the 70-85º range.

4. Discussion

Geometric constraints are generally held responsible for the supramolecular organization of dyes in ZL. The extent of these constraints depends on both the nature of the channels and the size, shape, and charge of the guests, as illustrated in Figure 1. Experiments have shown, that the cationic dye molecules Ox^+ and Py^+ are especially well suited guests for getting deeper insight into the microscopic nature and consequences of these constraints because they are of such a shape and size that different orientations inside the nanochannels, all compatible with the zeolite steric constraints, may be possible.[3,15,17,23,24] In this respect, our results suggest a key role of the competition between intermolecular interactions and interactions with the zeolite, whose relative strength ultimately governs the arrangement of the molecules inside ZL channels.

One of the most important results of our study is that the preferential orientation of Ox^+ in the composite is determined by the water co-solvent: whereas in the dry composite Ox^+ tends to align with the channel axis, the molecule prefers to stay perpendicular and confined into a single ZL unit cell in the presence of water. At the origin of this behaviour, emerging from both the optimized (0 K) structures and the room temperature simulations, lie two main factors, that may be addressed as "stabilization of the host", and "stabilization of the guest", respectively. They actually result from several concomitant and competing effects that, in general, concur to determine how molecules organize inside a nanosized porous matrix for a given set of conditions: In our case, the "host" is ZL with its extraframework cations content, the "guest" is Ox^+, and the presence/absence of water represents the "given set of conditions".

In the dry composite, the alignment of Ox^+ with the channel axis may be rationalized in terms of "stabilization of the guest". This means that the aligned orientation optimizes the Ox^+ interactions with the zeolite without perturbing its molecular geometry. First of all, in the parallel arrangement the distances between Ox^+ and K^+ are larger than in the structure with perpendicular Ox^+; as a consequence, the electrostatic repulsion between positively charged species inside the ZL channel is minimized. In addition, in the minimum energy structure Ox^+ is also stabilized by stronger Ox^+/ZL hydrogen bonds with the zeolite framework oxygens. Last but not least, distortion of the Ox^+ molecular structure from planarity is minimal in the aligned orientation.

On the other hand, "stabilization of the host" plays a dominant role in the wet composite because here the leading interactions are the water-zeolite ones. Indeed, owing to the greater number and strength of hydrogen bonds formed by water molecules with the zeolite, the stabilization of the host caused by hydration is energetically more important than the stabilization of Ox^+ by the water hydrogen bonding network. The perpendicular Ox^+ orientation not only maximizes the water-ZL interactions, but also keeps Ox^+ confined inside one ZL cage and leaves the maximum possible number of ZL unit cells occupied by water molecules in their energetically most favorable arrangement, as evidenced in Figure 8, where the minima of the **2c-ZL/Ox^+•24H_2O**

systems are shown. Such an optimal water organization is very similar to that found in the hydrated potassium-rich form of natural ZL, the zeolite perlialite, which features inside each cage 6-membered "rings" of water molecules interacting with both the channel walls and the potassium ions.[32c] This co-solvent organization is strongly perturbed by the presence of aligned Ox^+ molecules.

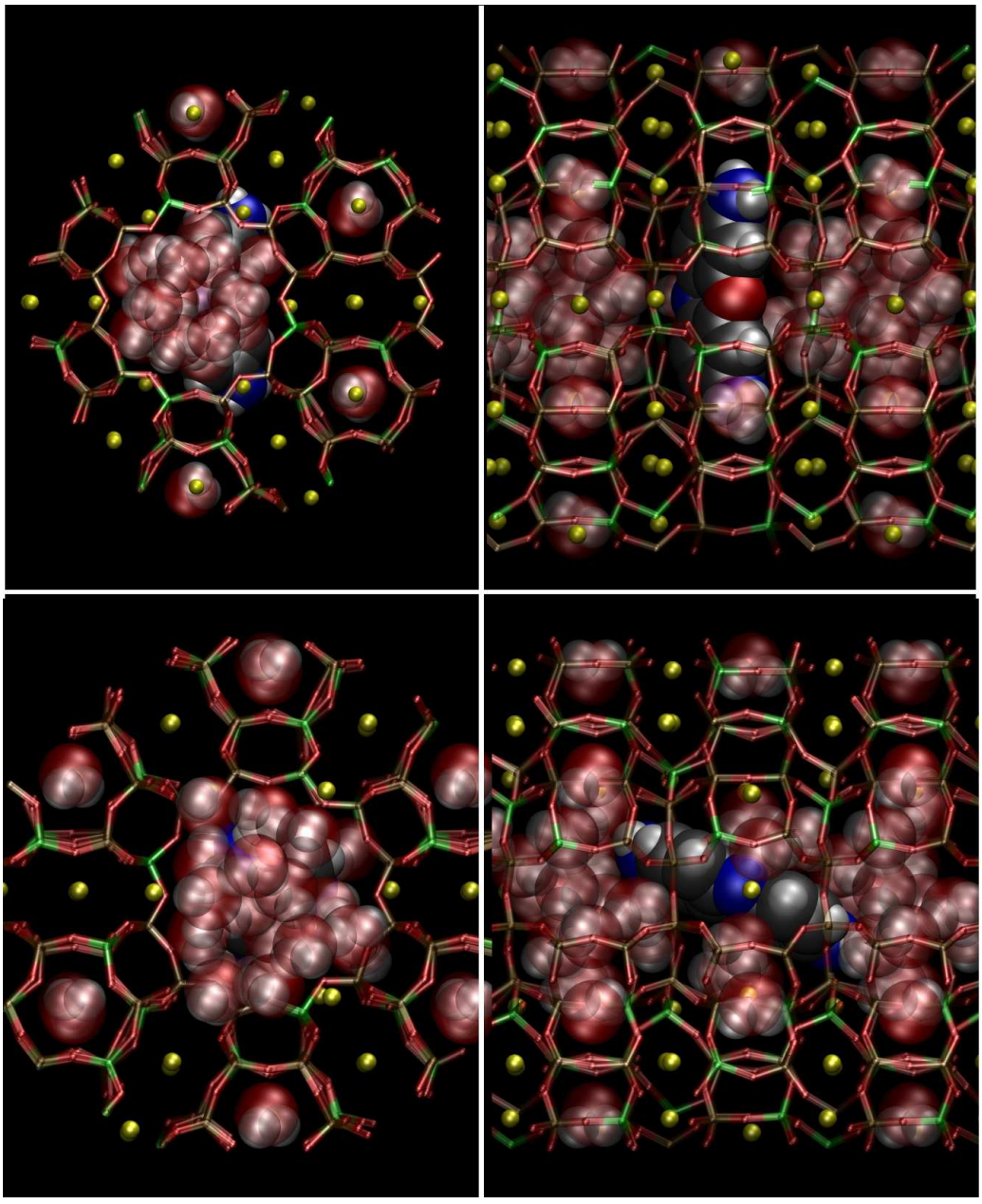

Figure 8. Spatial arrangement of dye and water molecules for the two alternative Ox^+ orientations in the 2c-ZL/Ox^+•24H_2O system projected on the ZL channel section (left) and along the channel direction

(right). Top panels: Minimum energy structure (Opt1, Table 2). Bottom panel: Opt2 (Table 2). Color codes: Al: green, Si: brown, O: red, K: yellow, N: blue, C: gray, H: white. Ox^+ and water atoms are represented as van der Waals spheres.

So far, the discussion refers to $Ox^{+/}$ZL composites only, since calculations were mainly carried out with Ox^+ as a guest. However, the same arguments should hold true for Py^+ as well in view of the results on Py^+/ZL, indicating that the small differences between these two dyes do not significantly affect the dye orientation inside ZL and its arrangement in the hydrogen bonding network of water.

It remains to understand how these results are related with the optical measurements. As reported in the introduction, a cone type distribution[23] or more precisely a cone-bell-shaped distribution[24] with a half-cone angle in the 72-80° range, with a margin of a few degrees, was deduced for both Ox^+ and Py^+. All experimental data refer to ambient temperature and humidity conditions under which the dye zeolite composites are hydrated. We found, in both of our computational investigations, energy minima and room temperature simulations, on dry and on hydrated Ox^+/ZL models, no evidence for a stable orientation of Ox^+ with a half-cone angle α in that range. Actually, several FPMD simulations/geometry optimizations were performed in which the starting configuration featured Ox^+ oriented in the 72-80° range; for example, the Opt5 and Opt6 optimizations in Table 2. However, upon equilibration/optimization such starting geometries always led to structures where Ox^+ was oriented either perpendicular to the ZL channel axis (Opt5, Movie 3 in the Supporting Information) or with α in the 40-55° range (Opt6, Movie 4 in the Supporting Information), the latter at higher energy. Such findings indicate that α = 70-85° is not an energetically favored orientation, and it might only be visited transiently by Ox^+ at room temperature. Altogether, these results suggest that different ways to interpret the optical microscopy data should be considered. Instead of interpreting the 70-85° half cone angle of Ox^+ as due to Ox^+ molecules oriented at α =70-85° with respect to the channel axis, one might think that this value actually derives from the superposition of differently oriented Ox^+. According to our calculations, in the hydrated system, which corresponds to the optical microscopy experiments conditions, the most stable orientation is 88°, however other conformations, with Ox^+ nearly aligned to the channel, are quite close in energy and can be easily accessed at room temperature. Following this argument, the actual distribution of Ox^+ inside the ZL channel should result from a larger portion of Ox^+ molecules perpendicularly oriented and a smaller fraction approximately aligned to the channel. The optical microscopy data might therefore be interpreted as the resultant, i.e., the "vector sum" of components arising from an Ox^+ population characterized by non uniform orientation,[47] mainly perpendicular to the channel but contaminated by a fraction of molecules approximately aligned to the channel. Indeed, such a minority fraction of nearly parallel Ox^+ could be responsible of the J-aggregates formation observed in ZL. Our new interpretation of optical data would therefore reconcile two seemingly contrasting observations and ultimately solve the conundrum of how J-aggregate formation in ZL, reported

for Py^+ and Ox^+ in refs. [19] and [17], respectively, could be compatible with the Ox^+ half-cone-angle deduced from optical experiments.

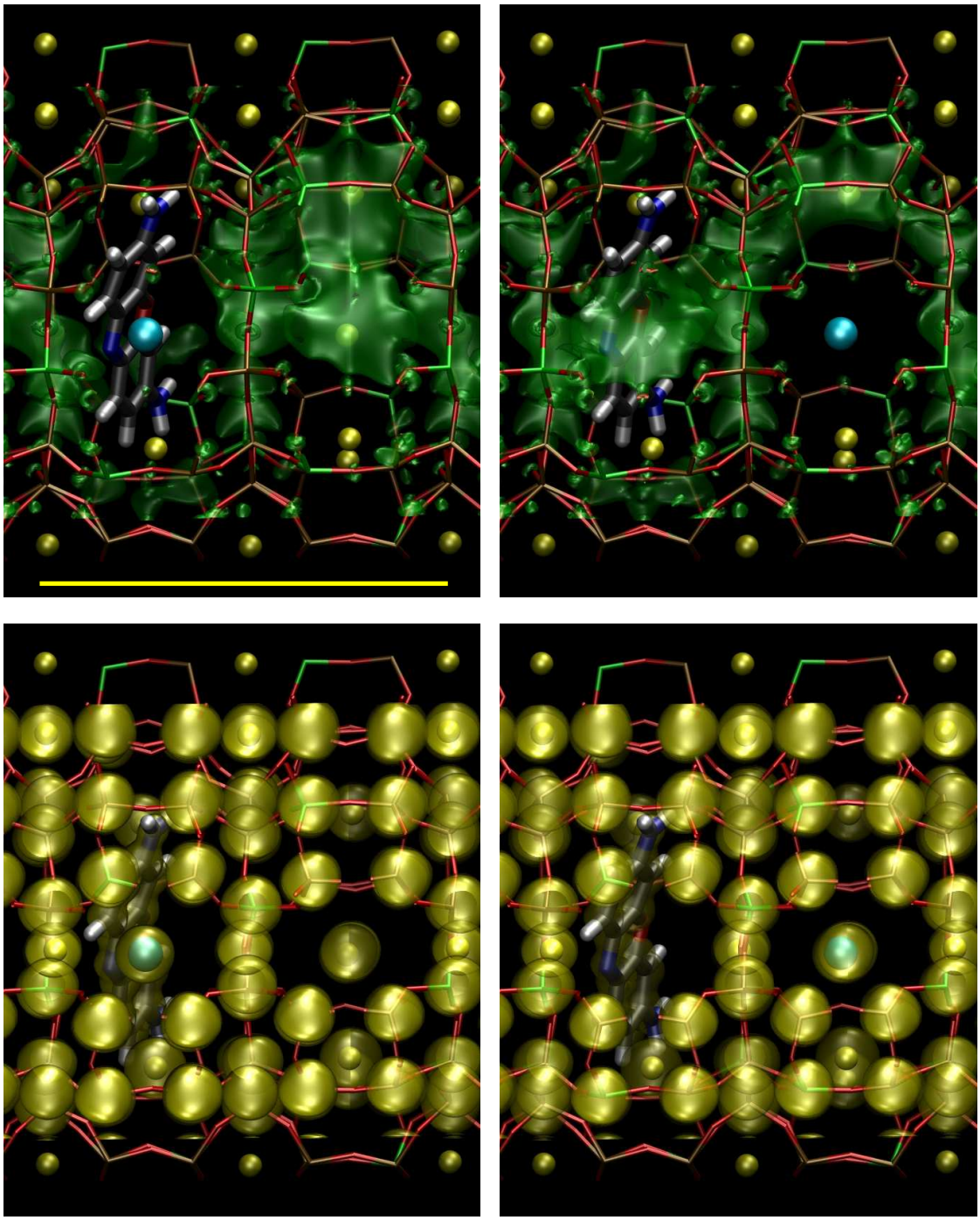

Figure 9: Electrostatic potential (EP) isosurface plots for the starting configuration of simulation D3 before (left panels) and after (right panels) the displacement of one K^+ (highlighted as a cyan sphere) from

the ZL cell containing Ox^+ to the adjacent cell. Top and bottom panels represent negative (green surface) and positive (yellow surface) EP regions, respectively. Atom color codes as in Figure 4. A yellow line in the top-left panel represents the simulation cell dimension along the channel.

In this respect, it is also worthy to stress that even though the parallel orientation is not the equilibrium arrangement for the hydrated Ox^+/ZL composite, the low mobility of Ox^+ in the presence of water makes it likely that a small though appreciable number of Ox^+ molecules could remain frozen in such an arrangement for quite long times, comparable with the optical experiments' timescales. Moreover, such a low Ox^+ mobility, detected along our simulations, is in line with the experimental observation that diffusion of Ox^+ inside ZL is very slow even at 100ºC.[48] Specifically, the energy barrier for Ox^+ diffusion deduced from kinetic data amounts to 18 kcal/mol, which is far beyond the energy of thermal fluctuations at room temperature conditions. These data, together with simulation results, suggest that it would be interesting to investigate experimentally Ox^+ diffusional and orientational behaviour in the presence of different solvents or in dry conditions.

Another general and relevant aspect emerging from our results is the flexibility of Ox^+ molecular structure, which allows for large fluctuations from the gas-phase π-system planar structure. In particular, simulations of both dry and hydrated Ox^+/ZL models showed that Ox^+ interactions with the host and with water molecules as well can induce transient distortions from planarity that might become significant at room conditions. On these basis, we suggest that molecular flexibility may also play a pivotal role in Ox^+ diffusion through ZL nanochannels.

Indeed, if one considers that, for entering in ZL and moving along its nanochannels, Ox^+ needs to be aligned to the channel axis, it still remains to understand how could Ox^+ achieve the perpendicular orientation inside one cell and how could it escape from such an orientation. Due to the high diffusion barrier at wet conditions, standard FPMD time scales may be too short to directly observe Ox^+ diffusional motion or net changes of orientation. In order to explore the molecular-level mechanism which allows Ox^+ to enter/escape from one cage in the presence of water, the combined use of statistical sampling techniques would be required,[49] and this will be the subject of future investigations. Some promising hints have been gathered by monitoring an escape of Ox^+ from the perpendicular orientation in the dry composite. As indicated by the energy difference with the corresponding minimum energy structure, the perpendicular orientation is actually a metastable state of the dry system. However, both steric constraints (i.e., Ox^+ "entrapment" into one ZL cell) and interactions with the host (electrostatics, dye-zeolite hydrogen bonds) effectively contribute to stabilize such an arrangement, thus making it difficult for 90º Ox^+ to figure out a reasonable way out. Therefore, we forced an escape event by means of a sudden charge unbalance, monitored Ox^+ dynamics and investigated how such a behaviour might be related with the host's electrostatic properties. Figure 9 shows the negative and positive

electrostatic potential (EP) regions of the ZL cell containing Ox^+ and of the adjacent one, before and after the displacement of a K^+ from the cell containing Ox^+ to the adjacent cell. It is evident that the displacement has both decreased the positive (i.e., unfavourable) EP close to Ox^+ and created a cage-shaped region of negative (i.e., favourable) EP around Ox^+, extending through the channel aperture to the adjacent cell, thus paving the way for Ox^+ escape through a "negative electrostatic potential path". The escape, however, actually occurs because of the dramatic "squid-like" distortion of the Ox^+ molecular structure. Such a deformation is, of course, induced by the charge unbalance, but it is also potentially intrinsic to the Ox^+ dynamical behaviour as it corresponds to its lowest frequency vibrational mode (see Supporting Information). Molecular flexibility, enhanced by electrostatic potential unbalances, and combined with ZL framework flexibility may therefore be one of the possible factors governing the Ox^+ enter-escape-reorientation mechanism.

5. Conclusions

The present study reveals that the orientation of Ox^+ and Py^+ xantene dyes inside zeolite L nanochannels depends on hydration and identifies the microscopic origin of this peculiar co-solvent-driven behavior, here unraveled for the first time. Radically different preferential orientations are obtained in the presence or absence of water because of the dominant stabilization of either the host or the guest, respectively. In particular, we highlighted that the perpendicular orientation of the dye molecule in the wet composite is favored because it implies a greater stabilization of the host, a crucial but frequently overlooked factor in the study of supramolecular organizations in nanosized matrices. The results here presented may help future studies on these systems to properly consider host stabilization. Moreover, the remarkable difference between the most stable orientations of the dye at dry and wet conditions suggests future work aimed at achieving atomistic-level control of this key aspect. A deeper understanding of the dependence of orientation from concentration of the dye and nature of the solvent could be achieved by designing and performing further experiments on Ox^+,Py^+/ZL materials in which loading is performed with different solvents, or even under dry conditions, as it has already been suggested in ref. [17]. In addition, time, space and spectrally resolved data on single crystals at different loading conditions, similar to those reported in refs. [17,19,20] but including anisotropy, could be of help in refining the interpretation of optical microscopy results. Furthermore, in light of the 'frictioned' dynamics of Ox^+ in the hydrated composite, and of its squid-like diffusion at dry conditions, here highlighted for the first time, it would be particularly interesting to see whether direct experimental observation of Ox^+ and/or Py^+ diffusion could be done on single crystals with sufficient spacial resolution. In a broader scenario, this study represents a significant advance in connecting experimental data to molecular behaviour in chemically complex systems like organic-inorganic hybrid composites and may contribute to inspire knowledge-based design and fabrication strategies for technologically appealing materials.

Acknowledgements

CINECA supercomputing center (Bologna, Italy) is gratefully acknowledged for computing time (ISCRA project 2011 “ZeoDye” HP10B8FNIH).

Supporting Information Available: Atomic coordinates and graphical representations of *ab initio* optimized geometries of isolated Ox^+ calculated with gaussian basis sets at different levels of theory, and corresponding first electronic excitation wavelength and ETDM calculated at different levels of theory. Atomic coordinates and graphical representations of optimized geometries of hydrated Ox^+ ($Ox^+ \bullet 6H_2O$) and of $Ox^+Cl^- \bullet 5H_2O$ and corresponding electronic excitation wavelength. ETDM orientation calculated from a configuration of the 2c-ZL/$Ox^+ \bullet 18H_2O$ W1 simulation. Graphical representation of the lowest energy vibrational mode of isolated Ox^+. Movies of the FPMD simulations of the dry and hydrated 2c- composites, Movie 1 and Movie 2, referring to the D4 and W2 simulations in the text, respectively. Movies of two geometry optimizations of the 2c-ZL/$Ox^+ \bullet 18H_2O$ composites (Movie 3 and Movie 4), referring to the Opt5 and Opt6 calculations, respectively (Table 2 of the main text). Optimized coordinates, graphical representations and binding energies of the $Ox^+ \bullet H_2O$ and $Py^+ \bullet H_2O$ complexes, with the water molecule coordinated to the central N of Ox^+ and to the central CH of Py^+, respectively. Full reference (38). This material is available free of charge via the Internet at http://pubs.acs.org

References and Notes

[1] (a) Marlow, F.; Caro, J.; Werner, L.; Kornatowski, J.; Dähne, S. *J. Phys. Chem.* **1993**, *97*, 11286-11290. (b) Caro, J.; Marlow, F.; Wübbenhorst, M. *Adv. Mater.* **1994**, *6*, 413-416. (c) *Host-Guest Systems based on Nanoporous Crystals*, ed. F. Laeri, F. Schüth, U. Simon and M. Wark, Wiley-VCH, Weinheim, **2003**. (d) Hisaki, I.; Murai, T.; Yabuguchi, H.; Shigemitsu, H.; Tohnai, N. ; Miyata, M., Crys. Growth Des. **2011**, 11, 4652-4659. (e) Garo, F.; Häner, R., *Angew. Chem. Int. Ed.* **2012**, *51*, 916-919. (f) Maggini, L; Bonifazi, D. *Chem. Soc. Rev.* **2012**, *41*, 211–241.

[2] (a) Schulz-Ekloff, G.; Wöhrle, D.; van Duffel, B.; Schoonheydt R. A. *Micropor. Mesopor. Mater.* **2002**, *51*, 91–138. (b) Bein T. in *Studies in Surface Science and Catalysis, Vol. 168: Introduction to Zeolite Science and Practice*, Eds. J. Cejka, H. van Bekkum, A. Corma and F. Schüth, Elsevier, Amsterdam, 3rd ed., **2007**, pp. 611–657. (c) Devaux, A.; Cucinotta, F.; Kehr, S.; De Cola, L., in *Functional supramolecular architectures for organic electronics and nanotechnology*. Eds. Samori, P.; Cacialli, F. Wiley **2011**, *Vol. 1***,** 283-342.

[3] (a) Calzaferri, G.; Huber, S.; Maas, H.; Minkowski, C. *Angew. Chem. Int. Ed.* **2003**, *42*, 3732-3758. (b) Calzaferri, G.; Pauchard, M.; Maas, H.; Huber, S.; Khatyr, A.; Schaafsma T. *J. Mater. Chem*. **2002**, *12*, 1-13. (c): Pauchard, M.; Devaux, A.; Calzaferri, G. *Chem. Eur. J.* **2000,** *6*, 3456-3470.

[4] (a) H. Sung Kim,S. M. Lee, K. Ha, C. Jung, Y.-J. Lee, Y. S. Chun, D. Kim, B. K. Rhee, K. B. Yoon *J. Am. Chem. Soc*. **2004**, 126, 673-682. (b) Kim, H. S.; Sohn, K. W.; Jeon, Y.; Min, H.; Kim, D.; Yoon, K. B. *Adv. Mater.* **2007**, *19*, 260–263. (c) Roeffaers, M. B. J. ; Ameloot, R. ; Baruah, M. ; Uji-i, H. ; Bulut, M.; De Cremer, G.; Müller, U. ; Jacobs, P. A.; Hofkens, J. ; Sels, B. F.; De Vos, D. E., *J. Am. Chem. Soc.* **2008**, *130*, 5763–5772. (d) van der Veen, M. A.; Valev, V. K.; Verbiest, T.; De Vos D. E., *Langmuir* **2009**, *25*, 4256-4261. (e) Inagaki, S.; Ohtani, O.; Goto, Y.; Okamoto, K.; Ikai, M; Yamanaka, K.; Tani, T.; Okada, T. *Angew. Chem. Int. Ed.* **2009**, *48*, 4042 –4046. (f) N. Gartmann, D. Brühwiler, *Angew. Chem. Int. Ed.* **2009**, *48*, 6354 –6356. (g) Pham, T. C. T.; Kim, H. S.; Yoon, K. B., *Science.* **2011**, *334*, 1533-1538.

[5] (a) Calzaferri, *Langmuir* **2012,** *28*, 6216-6231, dx.doi.org/10.1021/la3000872. (b) Brühwiler, D.; Calzaferri, G.; Torres, T.; Ramm, J. H.; Gartmann, N.; Dieu, L.-Q.; López-Duarte, I.; Martinez-Diaz, M. *J. Mater. Chem.* **2009**, *19*, 8040-8067.

[6] (a) P. J. Langley, J. Hulliger, *Chem. Soc. Rev.* **1999**, *28*, 279. (b) Chizhik, A. M.; Berger, R.; Chizhik, A. I.; Lyubimtsev, A.; Viani, L.; Cornil, J.; Bär, S.; Hanack, M.; Hulliger, J.; Meixner, A. J.; Egelhaaf, H.-J.; Gierschner J. *Chem. Mater.* **2011**, *23*, 1088–1090. (b) Winkler, R.; Berger, R.; Manca, M.; Hulliger, J.; Weber, E.; Loi, M. A.; Botta, C., *ChemPhysChem* **2012**, *13*, 96-98.

[7] (a) Ramamurthy, V.; Inoue, Y. *Supramolecular Photochemistry*, Wiley&Sons, **2011**, ISBN-13: 978-0-470-23053-4. (b) Freitag, M.; Galoppini, E. *Energy Environ. Sci.* **2011**, *4*, 2482-2494. (c) Babu, S.S.; Kartha, K. K.; Ajayagosh, A. *J. Phys. Chem. Letters* **2010,** *1*, 3413-3424.

[8] Albuquerque, R. Q.; Hofmann, C. C.; Köhler, J.; Köhler, A. *J. Phys. Chem. B* **2011**, *115*, 8063–8070.

[9] (a) Woerdemann , M.; Gläsener , S.; Hörner, F.; Devaux, A.; De Cola, L.; Denz, C. *Adv. Mater.* **2010**, *22*, 4176–4179. (b) Guerrero-Martinez, A.; Fibikar, S.; Pastoriza-Santos, I.; Liz-Marz, L. M.; De Cola, L. *Angew. Chem. Int. Ed.* **2009**, *48*, 1266-1770.

[10] (a) Hashimoto, S.; Hagiri, M.; Matsubara, N.; Tobita, S. *Phys. Chem. Chem. Phys.* **2001**, *3*, 5043-5051 (b) Hashimoto, S.; Uehara, K.; Sogawa, K.; Takada, M.; Fukumura, H. *Phys. Chem. Chem. Phys.* **2006**, *8*, 1451-1558. (c) Hashimoto, S.; Yamaji, M. *Phys. Chem. Chem. Phys.* **2008**, *10*, 3124-3130. (d) Hashimoto, S.; Samata, K.; Shoji, T.; Taira, N.; Tomita, T.; Matsuo, S., *Micropor. Mesopor. Mater.* **2009**, *117*, 220– 227. (e) Hashimoto, S. *J. Phys. Chem. Lett.* **2011**, *2*, 509-519.

[11] a) Ding, Y.; Wang, Y.; Li, Y.; Cao, P.; Ren, T. *Photochem. Photobiol. Sci* **2011**, *10*, 543-547. b) Wang, Y.; Yue, Y.; Li, H.; Zhao, Q.; Fang, Y.; Cao, P. *Photochem.Photobiol. Sci* **2011**, *10*, 128-132. c) Mech, A.; Monguzzi, A.; Cucinotta, F.; Meinardi, F.; Mezyk, J.; De Cola, L.; Tubino, R. *Phys. Chem. Chem. Phys.* **2011**, *13*, 5605-5609. (d) Li, H.; Cheng, W.; Wang, Y.; Liu, B.; Zhang, W.; Zhang, H. *Chem. Eur. J.* **2010**, *16*, 2125-2130.

[12] a) Vohra, V.; Calzaferri, G.; Destri, S.; Pasini, M.; Porzio, W.; Botta, C. *ACSNano* **2010**, *4*, 1409. b) Vohra, V.; Bolognesi, A.; Calzaferri, G.; Botta, C. *Langmuir* **2010**, *26*,1590.

[13] (a) López-Duarte, I.; Dieu, L.-Q.; Dolamic, I.; Martínez-Díaz, M. V.; Torres, T.; Calzaferri, G.; Brühwiler, D. *Chem. Eur. J.* **2011**, *17*, 1855-1862. (b) Albuquerque, R. Q.; Calzaferri, G. *Chem. Eur. J.* **2007**, *13*, 8938 – 8952.

[14] (a) Tsotsalas, M. M.; Kopka, K.; Luppi, G.; Wagner, S.; Law, M. P.; Schäfers, M.; De Cola, L. *ACSNANO* **2010** , *4*, 342-348**.** (b**)** Li, Z.; Luppi, G.; Geiger, A.; Josel, H.-P.; De Cola, L., *small* **2011**, *7*, 3193–3201. (c) El-Gindi, J.; Benson, K.; De Cola, L.; Galla, H.-J.; Kehr N. S. *Angew. Chem. Int. Ed.* **2012**, *51*, DOI: 10.1002/anie.201109144.

[15] (a) Calzaferri, G.; Lutkouskaya, K. *Photochem. Photobiol. Sci.* **2008**, *7*, 879–910. (b) Calzaferri, G.; Devaux, A. in *Supramolecular Photochemistry*, Eds. Ramamurthy, V.; Inoue, Y., Wiley&Sons **2011**, ISBN-13: 978-0-470-23053-4.

[16] (a) Wang, Y.; Li, H.; Feng, Y.; Zhang, H.; Calzaferri, G.; Ren, T. *Angew. Chem. Int. Ed.* **2010**, *49*, 1434-1438. (b) Cao, P.; Li, H.; Zhang, P.; Calzaferri, G., *Langmuir* **2011**, *27*, 12614-12620.

[17] Calzaferri, G.; Méallet-Renault, R.; Brühwiler, D.; Pansu, R.; Dolamic, I.; Dienel, T.; Adler, P.; Li, H.; Kunzmann, A. *ChemPhysChem* **2011**, *12*, 580-594.

[18] a) Davydov, A. S. *Usp. Fiz. Nauk* **1964**, *82*, 393 –448. b) Kasha, M.; Rawls, H. R.; El-Bayoumi, M. A. *Pure Appl. Chem.* **1965**, *11*, 371–392.

[19] Busby, M.; Blum, C.; Tibben, M.; Fibikar, S.; Calzaferri, G.; Subramaniam, V.; De Cola, L. *J. Am. Chem. Soc.* **2008**, *130***,** 10970-10976.

[20] Busby, M.; Devaux, A.; Blum, Ch.; Subramaniam, V.; Calzaferri, G.; De Cola, L. *J. Phys. Chem. C*, **2011**, *115*, 5974-5988.

[21] Calzaferri, G.; Brühwiler, D.; Meng, T.; Dieu, L.-Q.; Malinovskii, V. L.; Häner, R. *Chem. Eur J*, **2010**, *16*, 11289–11299.

[22] Hennessy, B.; Megelski, S.; Marcolli, C.; Shklover, V.; Bärlocher, Ch.; Calzaferri, G. *J. Phys. Chem. B* **1999**, *103*, 3340-3351.

[23] (a) Megelski, S.; Lieb, A.; Pauchard, M.; Drechsler, A.; Glaus, S.; Debus, C.; Meixner, A. J.; Calzaferri, G. *J. Phys. Chem.* B **2001**, *105*, 25-35. (b) Pauchard, M.; Huber, S.; Méallet-Renault, R.; Maas, H.; Pansu, R.; Calzaferri, G. *Angew. Chem. Int. Ed.* **2001**, *40*, 2839-2842.
[24] Gasecka, A.; Dieu, L.-Q.; Brühwiler, D.; Brasselet, S. *J. Phys. Chem. B*, **2010**, *114*, 4192 – 4198.
[25] (a) Hashimoto, S.; Samata, K.; Shoji, T.; Taira, N.; Tomita, T.; Matsuo, S. *Micropor. Mesopor. Mater.* **2009**, *117*, 220– 227. b) Lee, J. S. *Bull. Korean Chem. Soc.* **2010**, *31*, 2190 – 2194.
[26] a) Blum, C.; Cesa, Y.; Escalante, M.; Subramaniam, V. *J. R. Soc. Interface*, **2009**, *6*, S35–S43. b) Domke, K. F.; Day,J. P. R.; Rago, G.; Riemer, T.A.; Kox, M. H. F.; Weckhuysen, B.M.; Bonn, M. *Angew. Chem. Int. Ed.* **2012**, *51*, 1343–1347.
[27] a) Breck, D. W. *Zeolite Molecular Sieves*, John Wiley & Sons, NY, **1974**. b) Baerlocher, Ch.; Meier, W. M.; Olson, D. H. *Atlas of Zeolite Framework Types*, Elsevier, Amsterdam, **2001**, 5th edn. c) *International Zeolite Association*, http://www.iza-structure.org. d) Ohsuna, T.; Slater, B.; Gao, F.; Yu, J.; Sakamoto, Y.; Zhu, G.; Terasaki, O.; Vaughan, D. E.; Qiu, S.; Catlow, C. R. *Chem. Eur. J.* **2004**, *10*, 5031-5040. e) Zabala Ruiz, A.; Brühwiler, D.; Ban, T.; Calzaferri, G. *Monatsh. Chem.* **2005**, *136*, 77–89. (f) Brent, R.; Anderson, M. W. *Angew. Chem. Int. Ed.* **2008**, *47*, 5327-5330.
[28] Megelski, S.; Calzaferri, G. *Adv. Funct. Mater.* **2001**, *11*, 277–286.
[29] Jung, C.; Hellriegel, C.; Platschek, B.; Wöhrle, D.; Bein, T.; Michaelis, J.; Bräuchle, C. *J. Am. Chem. Soc*. **2007**, *129*, 5570-5579.
[30] Fois, E.; Tabacchi, G.; Calzaferri, G. *J. Phys. Chem. C* **2010**, *114*, 10572 – 10579.
[31] Perdew, J. P.; Burke, K.; Ernzerhof, M., *Phys. Rev. Lett*. **1996**, *77*, 3865-3868.
[32] (a) Newsam, J.M., *J. Phys. Chem.* **1989,** *93*, 7689-7694; . (b) Barrer, R.M.; Villiger, H. *Z. Kristallogr.* **1969**, *128*, 352-370 ; (c) Artioli, G.; Kvick, Å. *Eur. J. Mineral*. **1990**, *2*, 749-759.
[33] (a) Vanderbilt, D. *Phys. Rev. B* **1990**, *41*, 7892-7895. (b) Kleinman, L.; Bylander, D.M. *Phys. Rev. Lett.* **1982**, *48*, 1425-1428. (c) Hamman, D. R.; Schlüter, M.; Chiang, C. *Phys. Rev. Lett.* **1979**, *43*, 1494−1497. (d) N. Troullier and J. L. Martins, Phys. Rev. B 43, 1993 (1991).
[34] (a) Gamba, A.; Tabacchi, G.; Fois, E. *J. Phys. Chem A* **2009**, *113*, 15006-15015. (b) Tilocca, A., Fois, E. *J. Phys. Chem C* **2009**, *113*, 8683-8687. (c) Fois, E.; Tabacchi, G.; Barreca, D.; Gasparotto, A.; Tondello, E., *Angew. Chem. Int. Ed.*, **2010**, *49*, 1944-1948.
[35] (a) Car, R.; Parrinello, M., *Phys. Rev. Lett*. **1985,** *55*, 2471-2475. (b) Marx, D.; Hutter, J. *Ab Initio Molecular Dynamics*, Cambridge University Press **2009**. (c) CPMD code, MPI für Festkörperforschung: Stuttgart, Germany; IBM Zürich Research Laboratory: Zürich, Switzerland, 1990−2012, www.cpmd.org.
[36] Frank, I.; Hutter, J.; Marx, D.; Parrinello, M. *J. Chem. Phys*. **1998**, *108*, 4060-4070.
[37] Fois, E.; Gamba, A.; Medici, C.; Tabacchi, G. *ChemPhysChem* **2005**, *6*, 1917-1922.
[38] Frisch, M. J. *et al.* Gaussian 09, Revision D.02; Gaussian, Inc.: Wallingford, CT, **2009**.

[39] Coudert, F.-X.; Cailliez, F.; Vuilleumier, R.; Fuchs, A.H.; Boutin, A., *Faraday Discuss*., **2009,** *141*, 377-398.
[40] (a) Trudu, F.; Tabacchi, G.; Gamba, A.; Fois, E. *J. Phys. Chem. C* **2008**, *112*, 15394-15401. (b) Fois, E.; Gamba, A.; Trudu, F.; Tabacchi, G. *Il Nuovo Cimento* **2008**, *123B*, 1567-1474; (c) Trudu, F.; Tabacchi, G.; Gamba, A.; Fois, E. *J. Phys. Chem. A* **2007**, *111*, 11626-11637.
[41] Fois, E.; Gamba, A.; Tabacchi, G., *ChemPhysChem* **2008**, *9*, 538-543.
[42] Spanò, E.; Tabacchi, G.; Gamba, A.; Fois, E. *J. Phys. Chem. B* **2006**, *110*, 21651-21661.
[43] Fois, E.; Gamba, A.; Spanò, E.; Tabacchi, G. *J. Mol. Struct.* **2003**, *644*, 55-66.
[44] Tabacchi, G.; Gamba, A.; Fois, E. (2009). Intracage Chemistry in Zeolitic Systems: The Car-Parrinello Approach. In: Basiuk V.A., Ugliengo P., eds., *Quantum Chemical Calculations of Surfaces and Interfaces of Materials*. p. 65-87; American Scientific Publishers: Stevenson Ranch, California, 2009. ISBN/ISSN: 1-58883-138-8.
[45] (a) Fois, E.; Gamba, A.; Tabacchi, G.; Quartieri, S.; Vezzalini, G. *J. Phys. Chem. B* **2001**, *105*, 3012-3016; (b) Fois, E.; Gamba, A.; Tabacchi, G.; Quartieri, S.; Vezzalini, G. *Phys. Chem. Chem. Phys.* **2001**, *3*, 4158-4163; (c) Fois, E.; Gamba, A.; Tabacchi, G.; Arletti, R.; Quartieri, S.; Vezzalini, G. *Stud. Surf. Sci. Catal*., **2005**, *155*, 271-280.
[46] (a) Quartieri, S.; Sani, A; Vezzalini, G.; Galli, E.; Fois, E.; Gamba, A.; Tabacchi, G. *Microp. Mesop. Mater.* **1999**, *30*, 77-87; (b) Fois, E.; Tabacchi, G.; Quartieri, S.; Vezzalini, G. *J. Chem. Phys.* **1999**, *111*, 355-359; (c) Fois, E.; Gamba, A.; Tabacchi, G.; Ferro, O.; Quartieri, S.; Vezzalini, G. *Stud. Surf. Sci. Catal.* **2002**, *142*, 1877-1884; (d) Ferro, O.; Quartieri, S.; Vezzalini, G.; Fois, E.; Gamba, A.; Tabacchi, G. *Am. Mineral.* **2002**, *87*, 1415-1425; (e) Fois, E.; Gamba, A.; Tabacchi, G. *ChemPhysChem* **2005**, *6*, 1237-1239; (f) Fois, E.; Gamba, A.; Tabacchi, G.; Arletti, R.; Quartieri, S.; Vezzalini, G. *Am. Mineral.* **2005**, *90*, 28-35; (g) Tabacchi, G.; Gianotti, E.; Fois, E.; Martra, G.; Marchese, L.; Coluccia, S.; Gamba, A. *J. Phys. Chem. C* **2007**, *111*, 4946-4955; (h) Betti, C.; Fois, E.; Mazzuccato, E.; Medici, C.; Quartieri, S.; Tabacchi, G.; Vezzalini, G.; Dmitriev, V. *Microp. Mesop. Mater.* **2007**, *103*, 190-209; (i) Fois, E.; Gamba, A.; Medici, C.; Tabacchi, G.; Quartieri, S.; Mazzuccato, E.; Arletti, R.; Vezzalini, G.; Dmitriev, V. *Microp. Mesop. Mater.* **2008**, *115*, 267-280.
[47] Scholes, G.D.; Jordanides, X. J.; Fleming, G. R., *J. Phys. Chem. B* **2001**, *105*, 1640-1651.
[48] Pfenniger, M.; Calzaferri, G. *ChemPhysChem* **2000**, *1*, 211-217.
[49] (a) Carter, E. A.; Ciccotti, G.; Hynes, J. T.; Kapral, R., *Chem. Phys. Lett.* **1989**, *156*, 472-477. (b) Fois, E.; Gamba, A.; Tabacchi, G., *Chem. Phys. Lett.* **2000**, *329*, 1-6. (c) Ceriani, C.; Fois, E.; Gamba, A.; Tabacchi, G.; Ferro, O.; Quartieri, S.; Vezzalini, G., *Am. Mineral.* **2004**, *89*, 102-109. (d) Tabacchi, G.; Zucchini, D.; Caprini, G.; Gamba, A.; Lederer, F.; Vanoni, M.A.; Fois, E. *FEBS J.* **2009**, *276*, 2368-2380; (e) Barreca, D.; Fois, E.; Gasparotto, A.; Seraglia, R.; Tondello, E.; Tabacchi, G. *Chem. Eur. J.* **2011**, *17*, 10864-10870.

TOC image: